J Nanopart Res (2020) 22: 347
https://doi.org/10.1007/s11051-020-05072-6

RESEARCH PAPER

Impact of the PtO loading on mesoporous TiO_2 nanoparticles for enhanced photodegradation of Imazapyr herbicide under simulated solar light

I. A. Mkhalid · J. L. G. Fierro · R. M. Mohamed · A. A. Alshahri

Received: 29 June 2020 / Accepted: 27 October 2020 / Published online: 9 November 2020
© Springer Nature B.V. 2020

Abstract The removal of the commonly used herbicides is essential for environmental remediation. In this study, mesoporous TiO_2 photocatalysts modified with PtO were synthetized by the template-assisted scheme to develop highly effective materials for the elimination of Imazapyr herbicide under visible-light preservation. The effect of the PtO loading was investigated, and the xPtO-TiO_2 materials were deeply considered by N_2 physisorption, XRD, HRTEM, FTIR, DRS UV-Vis, Raman, XPS, PL and photocurrent measurements. Total Imazapyr photodegradation was archived on mesoporous TiO_2 photocatalysts loaded with 0.6 and 0.8 wt% of PtO. The optimized xPtO-TiO_2 photocatalyst degrades the Imazapyr under solar light more efficiently than the pure TiO_2 and the commercial Degussa P25 (photoefficiency of 35%, 1%, and 0.5%, respectively). The improvement in the photoefficiency of the *x*PtO-TiO_2 photocatalysts respect to the pure TiO_2 was associated to the cooperative effect between PtO and TiO_2 nanoparticles leading to a lessening in the energy gap and lower recombination of excited electron-hole pairs. The optimized 0.6PtO-TiO_2 photocatalyst demonstrated to be stable and recyclable after up to five consecutive photocatalytic runs. Therefore, it can be a potential candidate for the significant mineralization of Imazapyr herbicide under solar light irradiation.

Keywords Mesoporous TiO_2 · PtO · Photocatalyst · Photodegradation · Imazapyr

This article is part of the topical collection: Nanotechnology in Arab Countries

Guest Editor: Sherif El-Eskandarany

I. A. Mkhalid (✉) · R. M. Mohamed · A. A. Alshahri
Department of Chemistry, Faculty of Science, King Abdulaziz University, P. O. Box 80203, Jeddah 21589, Kingdom of Saudi Arabia
e-mail: imkhalid2@gmail.com

J. L. G. Fierro
Sustainable Energy and Chemistry Group, Instituto de Catálisis y Petroleoquímica, CSIC, Marie Curie, 2 Cantoblanco, 28049 Madrid, Spain

R. M. Mohamed
Advanced Materials Department, Central Metallurgical R&D Institute, CMRDI, P.O. Box 87, Helwan, Cairo 11421, Egypt

Introduction

Imazapyr, of the imidazolinone family, is considered as non-selective herbicide which can regulate the plant growth of a broad scope of weeds (Pretzer et al. 2008). However, broad application of Imazapyr in the agricultural area brings about a significant environmental problem; primarily, it is known for its ease diffusion to the groundwater (Streal and Horner 2000). Indeed, Imazapyr was detected in drinking water at concentrations above the permitted concentration value (PCV) specified by the European Union (< 0.1 μg/L). To solve this problem, numerous attempts have been made to design efficient and low-cost treatments for herbicides destruction (Souza et al. 2014). In particular, adsorption

and chemical or electrochemical oxidation methods were deeply investigated for the Imazapyr elimination (Streal and Horner 2000; Souza et al. 2014). In the oxidation techniques, the best results were obtained using popular oxidizing agents such as chlorine, ozone, and chlorine dioxide. Besides the remarkable efficacy of the chemical oxidation techniques, their use led to the formation of secondary products which are harmful to the aquatic environment, mainly when applied for destruction of complex organic compounds. Therefore, the challenge is the elimination of those secondary, hazardous products (Mohamed et al. 2017). Alternatively, other oxidation processes could be adopted instead of the chemical oxidation methods. In this sense, recent investigations are focused on the use of advanced oxidation processes (AOPs), which demonstrated to be exceedingly useful for the complete oxidation of toxic compounds in aquatic environments via the generation of potent oxidizing agents, such as the hydroxyl (OH•) or superoxide (O_2^-) radicals with very high oxidation potentials (2.8 and − 2.4 V respectively) (Mohamed 2009; Atitar et al. 2015).

There is an extensive literature body demonstrating that elimination of the harmful organic contaminants in wastewaters can be archived via advanced oxidation processes using photocatalysts (Robben et al. 2012; Mohamed and Aazam 2013; Mohamed et al. 2012; Ismail et al. 2006). In this sense, numerous formulations have been investigated to obtain photocatalysts systems with high efficiency and minimal cost. Among the different catalyst formulations, the n-type TiO_2 semiconductor was one of the most studied owing to its photocatalytic efficiency under UV irradiation, exceptional chemical stability and resistance to photocorrosion, non-toxic nature, and low cost. Indeed, the TiO_2-based photocatalysts were successfully used for the elimination of toxic organic wastes owing to its high oxidizing capability upon UV irradiation (Ismail and Ibrahim 2008; Wang et al. 2009). In particular, exceptionally high photocatalytic properties have been found for mesoporous TiO_2-based photocatalysts with respect to that based on non-porous particulate systems (Atitar et al. 2015; Mohamed and Aazam 2013; Wang et al. 2009). Despite the photocatalytic advantages of mesoporous TiO_2, its main disadvantage is related to its high energy bandgap (3.2 eV) that bounds its efficiency under visible light irradiation. Thus, the challenge is to adjust the electronic possessions of TiO_2 to improve its efficiency for solar light application. Recently, a variety of different metal ions have been applied to dope and adapt the electronic properties of oxide-based photocatalysts (Pretzer et al. 2008; Mohamed and Aazam 2013; Ismail et al. 2016a). In this sense, the effect of the decoration of mesoporous TiO_2 with non-metal ions or transition metal ions has been extensively investigated (Tayade et al. 2006; Ishibai et al. 2007; Jing et al. 2005). Also, the alteration of TiO_2 with different oxide nanoclusters has been a successful tactic to improve the efficiency of TiO_2-based photocatalysts (Nolan 2011). Recently, promising results have been reported for the photocatalytic elimination of Imazapyr herbicide over mesoporous TiO_2 modified with various oxides (Ismail et al. 2015, 2016, 2018; Mkhalid et al. 2020). All those catalysts exhibited higher photocatalytic efficacies toward photooxidation of Imazapyr than non-mesoporous TiO_2 Degussa P25 photocatalyst.

In particular, optimistic results were obtained by the surface decoration of TiO_2 with platinum oxide species (Ishibai et al. 2007; Kibombo et al. 2013). However, the photocatalytic efficiency of the Pt-modified TiO_2 composites strongly depends on the oxidation of the platinum sorts (Mohamed et al. 2019; Kibombo et al. 2013). Among the different platinum oxides (Pt^{2+} and Pt^{4+}), the best photocatalytic results were obtained when TiO_2 was decorated with highly dispersed PtO nanoclusters (Ishibai et al. 2007; Kibombo et al. 2013). For example, TiO_2 nanocomposite decorated with PtO was successfully employed for the photooxidation of nitric oxide beneath visible light owing to its upgraded photonic efficacy (Ishibai et al. 2007) and the improved surface aspects when comparing to that of individual PtO and TiO_2 materials (Kibombo et al. 2013). As compared with anatase (3.2 eV), the PtO exhibits the conduction band at similar potential (Yang et al. 2012). This means that TiO_2 in close contact with PtO nanoclusters may facilitate the easy transferal of the generated electrons at the conduction band (CB) of TiO_2 to the CB of PtO. However, the use of PtO-TiO_2 photocatalysts in other photocatalytic processes, as photodegradation of harmful organic contaminants, is still scarce (Kibombo et al. 2013). In addition, the preparation of PtO nanoclusters includes complex stages and the photocatalytic action attained is quiet sensible resulting from the low crystallinity and dispersion of the PtO clusters (Wang et al. 2018).

Within this scenario, the purpose of this effort is the synthesis of TiO_2 modified vary amount of PtO nanoparticles with small size and high crystallinty through a

simple sol-gel synthesis method. The photocatalytic efficiency of the synthetized nanocomposites has been evaluated in the photocatalytic destruction of Imazapyr herbicide under solar light illumination using as references a commercial Degussa P25 TiO_2 and synthetized mesoporous TiO_2 catalysts. The physico-chemical properties of the synthetized PtO-TiO_2 photocatalysts have been explored by the diversity of systems to explain the influence of PtO loading on the catalyst photoefficiency.

Chemicals and experimental

Materials

All starting solvents and reagents (glacial acetic acid > 99%, hydrochloric acid 36.5–38.0%, potassium nitrate > 99%, absolute ethanol, and methanol > 99%) were bought from Sigma–Aldrich and used deprived of additional decontamination. Titanium (IV) tert-butoxide, [$Ti(OC(CH_3)_3)_4$, (TBOT), deposition grade] and tetraammineplatinum (II) nitrate 99.995% trace metals basis, were used as TiO_2 and PtO precursors respectively, while triblock copolymer F127 (EO_{106}-$PO_{70}EO_{106}$, M.W. 12,600 g/mol) was employed in the photocatalyst preparation as a surfactant and template.

Synthesis of mesostructured PtO-TiO_2 photocatalysts

Mesoporous PtO-TiO_2 photocatalysts with variable load of PtO (0.2, 0.4, 0.6, and 0.8 wt.%) were synthetized by template-assisted sol-gel method. Pure mesoporous TiO_2 reference was prepared by the same methodology as published in our previous work (Mkhalid et al. 2020). Briefly, the following steps were done to obtain the final photocatalysts. Firstly, a polymeric solution was made dispersing the F127 triblock copolymer (1.6 g) in ethanol (30 mL) under continuous stirring for 60 min. Then, the mesophase was prepared by slow addition of TBOT (3.5 mL), HCl (0.74 mL), and CH_3COOH (2.3 mL) to the previously prepared F127 polymer solution. This mesophase solution was kept upon magnetic stirring for 1 h until it reached perfect homogeneity. After this, the required amount of $Pt(NH_3)_4(NO_3)_2$ was introduced into the mesophase solution upon continuous magnetic stirring for 1 h. The resulting system was left for aging at 40 °C for 12 h in a chamber having 80% of humidity. After that, the obtained materials were left to dry overnight at 65 °C to permit ethanol evaporation and mesophase polymerization. Finally, the xerogel was heated in air at 500 °C for 4 h. The PtO-TiO_2 photocatalysts will be labeled hereafter as xPtO-TiO_2 (where $x = 0.2$, 0.4, 0.6 and 0.8 PtO wt%).

Photocatalyst characterization

The textural properties of the xPtO-TiO_2 photocatalysts were assessed from nitrogen adsorption isotherms using a Quanta-chrome machine. The BET technique intended the surface area, and sorption statistics were obtained by applying Halsey mathematical expression to Barrett-Joyner-Halenda (BJH) way (Gregg and Sing 1982). The nanomorphological structure of the photocatalysts was investigated using high-resolution transmission electron spectroscope (HR-TEM) using a JEOL JEM 2000FX (Japan) microscope operating at a maximum of 0.2 MV. The crystalline structure and phases identification were investigated through powder X-ray diffraction (XRD) utilizing a Bruker axis D8 XRD diffractometer (Germany) and Cu Kα ($\lambda = 0.15406$ nm) radiation. Fourier transform infrared spectra (FTIR) in the range 4000–400 cm^{-1} were noted on a Perkin-Elmer spectrophotometer by blending potassium bromide with the sample in the proportion of 100:1. Raman spectra were recorded via a Horiba LabRAM Aramis spectrometer using a 532 nm laser beam.

The surface characterization of the xPtO-TiO_2 photocatalysts was examined thru X-ray photoelectron spectroscopy (XPS) consuming a VG Escalab 200R apparatus having an Mg Kα X-ray source and hemispherical electron analyzer. The binding energy of the adventitious carbon C1s peak at 284.8 eV was used as a reference. The optical properties of the synthetized photocatalysts were detailed ambience in the range 200~800 nm using a Jasco (Japan) UV-Vis spectrophotometer. The optical bandgap energies were investigated using the Kubelka–Munk formula and Tauc plot (Tauc et al. 1966). Photoluminescence emission spectra (PL) were dignified in the scan range 300–900 nm by a luminescence RF-5301 spectrophotometer (Shimadzu) and a quartz cuvette of 1 cm^{-1} path distance. The sample ultrasonically spread in ethanol was familiarized into a cuvette and open to simulated solar light irradiation with a 300 W Xe lamp. Electrochemical work station (Zahner Zennium) was employed to register the transient photocurrent under light on-off states.

Photocatalytic tests for Imazapyr degradation

Imazapyr herbicide was selected as a prototypical pollutant molecule to assess the photocatalytic efficacy of the synthetized trials. Photocatalytic activity of the pure TiO_2 and *x*PtO-TiO_2 samples was evaluated at room temperature using a borosilicate glass reactor beneath pretend solar light lighting (300 W Xe lamp; emission intensity of 2 $mW{\cdot}cm^{-2}$). The detachment concerning the exterior of Imazapyr target and illumination lamp was 10 cm. The amount of photocatalyst was dispersed into 50 mL of water (1.0 g/L) and ultrasonically sonicated in the dark for 15 min. Then, KNO_3 (10 mmol/L) was added to the photocatalyst suspension to retain constant ionic forte of the solution and to minimize the effect of HCl, which is used to obtain pH value of 3. Then, a stock of Imazapyr solution with a concentration of 7.65 mmol/L was prepared. For each photocatalytic test, the calculated volume of the Imazapyr solution was withdrawn from the stock solution to achieve the required Imazapyr concentration in the reactor (0.08 mmol/L). Before irradiation, the suspension was regimented under incessant rousing in the dark at 27 °C for 3 h to archive the Imazapyr adsorption-desorption equilibrium. The examination of Imazapyr concentration was achieved in a High Recital Liquid Chromatography of Agilent apparatus equipped with UV detector. The HPLC tool workings were applying two phases; (i) motionless phase of an Agilent Eclipse Plus C_{18} column (110 mm length, 4.8 mm id; particles of 3.5 μm diameter) and (ii) mobile phase containing H_3PO_4 and methanol/water combination (30:70% v/v). The retention time of the HPLC analysis was of 4.6 min, whereas the stream rate was adapted at a constant rate (0.8 mL min^{-1}). The calibration of the pollutant concentrations (0 to 0.8 mmol L^{-1}). For analysis, a certain quantity of suspension was engaged at unvarying time interims. The analysis of the suspension was made prior to and after the illumination process. The mineralization of Imazapyr was studied utilizing a UV-persulfate TOC tester for the measurement of total organic carbon (TOC). The photocatalytic efficiency of the synthetized photocatalysts have been equated with that of a commercial Degussa P25 TiO_2 photocatalyst (anatase: rutile as 3:1; 50 m^2 g^{-1}, Sigma-Aldrich).

Results and discussion

Photocatalyst depiction

X-ray diffractograms of the pure TiO_2 and xPtO–TiO_2 powders are exposed in Fig. 1. The XRD patterns of all synthetized photocatalysts show Bragg reflections peaks of low intensity at $2\theta = 25.4°$, 36.4°, 48.1°, 54.2°, and 62.8° corresponding to the (101), (004), (200), (211), and (213) crystalline reflections correspondingly of anatase TiO_2 phase (JCPDS 21–1272) (Vargas et al. 1999; Cardenas-Lizana et al. 2009; Shannon 1976; Kumaresan et al. 2011; Faisal et al. 2014; Ismail et al. 2009; Sekiya et al. 2001). Neither the intensity, the width, nor the position of the diffraction peaks of the anatase phases in the PtO–TiO_2 photocatalysts are modified with respect to the pure TiO_2 which indicated that the nucleation, growth, and crystallization of the TiO_2 during the sol-gel synthesis are scarcely affected by the presence of Pt^{2+} ions. Noticeably, all the PtO-TiO_2 photocatalysts does not show diffraction peaks associated neither with Pt nor PtO crystalline phases. This is probably because of the low PtO loading (0.2–0.8 wt%) that leads to Pt crystallites of low size below the detection limit of the XRD technique.

Further evidence about the state of the Pt sorts in the synthetized xPtO–TiO_2 photocatalysts was obtained from both Raman and FTIR spectroscopies. Figure 2a displays the Raman spectra of the synthetized xPtO-TiO_2 samples and pure TiO_2 reference. The Raman spectra of all samples show well-defined six bands located at 519 cm^{-1} (A_{1g} and B_{1g} modes of anatase), 399 cm^{-1} (B_{1g}), and 144 cm^{-1} (E_g) which are typical of the fundamental modes of the anatase phase indicating that the TiO_2 in the xPtO-TiO_2 photocatalysts consists of anatase nanocrystals (Acosta-Silva et al. 2013). Additionally, the pure TiO_2, 0.2PtO-TiO_2, and 0.4PtO-TiO_2 trials exhibit the band at 448 cm^{-1} (E_g) suggesting the presence of small crystallites of the rutile phase which were not noticed via XRD (Mkhalid et al. 2020). On the opposing, the rutile phase was absent in the 0.6PtO-TiO_2 and 0.8PtO-TiO_2 samples. Regarding the possible incorporation of Pt within the lattice of TiO_2, it could be discarded because the changes in the Pt loading does not alter the Raman spectra of pure TiO_2 reference; only a decrease in the intensity as the platinum content in the photocatalysts increased, in good agreement with previous XRD analysis. The surface groups present on the TiO_2 and PtO-TiO_2 photocatalysts

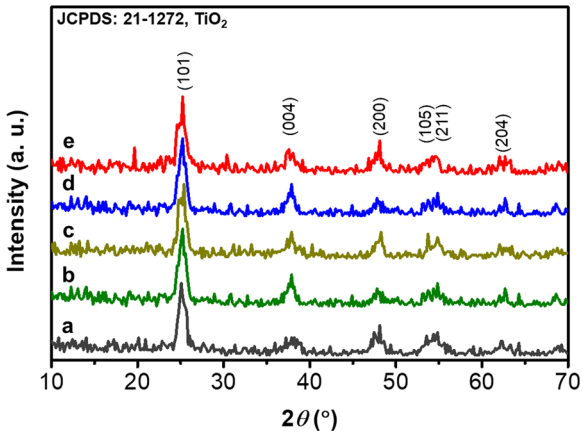

Fig. 1 X-ray diffraction analysis of pure TiO_2 (**a**) and *x*PtO-TiO_2 photocatalysts: 0.2PtO-TiO_2 (**b**), 0.4PtO-TiO_2 (**c**), 0.6PtO-TiO_2 (**d**), and 0.8PtO-TiO_2 (**e**)

were studied by FTIR spectroscopy (Fig. 2b). The general features of all photocatalysts are similar, showing a broadband at 3350–3600 cm^{-1} range associated with adsorbed water molecules on the hydroxyl groups of TiO_2 (Ti-OH) (Sekiya et al. 2001). Indeed, the height positioned at 1626 cm^{-1} could be allocated to vibrations modes (bending type) of H_2O molecules that are physically adsorbed on the TiO_2 surface (Faisal et al. 2014). The wide absorption band among 500~800 cm^{-1} are mostly credited to Ti-O and O-Ti-O vibrations (Ismail et al. 2009). No apparent shift in the extending vibration of Ti–O in the xPtO-TiO_2 photocatalysts was observed with respect to the pure TiO_2 reference, discarding, therefore, any Pt doping on the external of TiO_2. On the other hand, the uttermost at a wavenumber of 560–570 cm^{-1} could also include the vibrational mode of the bonds between Pt and oxygen (Pt-O) suggesting the increase in intensity in the xPtO-TiO_2 photocatalysts formation of Pt-O bonds (Acosta-Silva et al. 2013). Finally, there is no evidence of the presence of vibrational modes (bending and stretching) of C-H bond groups confirming the successful and complete removal of F127 triblock copolymer during the calcination step.

The formation of mesoporous structure in the pure TiO_2 and *x*PtO-TiO_2 photocatalysts was confirmed from the N_2 adsorption-desorption measurements at − 196 °C, showing all samples a high specific BET surface area (S_{BET}) = 155–170 m^2/g (Table 1). Despite the low PtO loading (0.2–0.8 wt.%), the particular BET surface areas reduced with the surging the Pt in the *x*PtO-TiO_2 nanocomposites. The decrease in the S_{BET} of the catalyst with the Pt loading suggests different porous structure and/or the pores mounts blocked by well-dispersed platinum particles. However, there is no observable alteration in the nitrogen adsorption properties over the synthetized *x*PtO-TiO_2 photocatalysts suggesting that the modification of TiO_2 with platinum nanoparticles does not destroy the porous structure of the pureTiO_2. More information can be obtained by comparison of isotherms of the 0.6PtO-TiO_2 sample, representing the *x*PtO-TiO_2 photocatalysts, to those of the bare TiO_2 (Fig. 3). As can be seen, both catalysts exhibited type IV isotherm. Their hysteresis loop of H3 type is typical of mesoporous materials with random pore structures. The hysteresis loop of the 0.6PtO-TiO_2 sample catalyst decreased concerning the pure TiO_2 sample indicating a decrease of the pore volume, in good agreement with the S_{BET} trend. As compared with pure TiO_2, the hysteresis loop of 0.6PtO-TiO_2 is shifted toward lower values of relative pressures indicating that this sample possesses a more significant amount of mesoporous than pure TiO_2. Noticeably, the macropores are absent in the 0.6PtO-TiO_2 sample, as deduced from the plateau of the adsorption curve at high relative pressure region, which is typical of multilayer adsorption on the external catalyst surface. Thus, the lower S_{BET} of the *x*PtO-TiO_2 samples concerning pure TiO_2 was probably linked to the loss of macropores blocked with the increase of the loading of platinum nanoparticles.

The nanomorphology of the *x*PtO-TiO_2 photocatalysts (represented by the 0.6PtO-TiO_2 sample) analyzed by transmission electron microscopy was compared to bareTiO_2. Figure 4a and b collects the electron micrographs of the 0.6PtO-TiO_2 and pure TiO_2 samples respectively showing both samples the presence of TiO_2 crystallites with similar nanomorphology (regular rhombohedra and cube contours) and particle size (in the 8–10 nm range). The high magnification images (HRTEM) of TiO_2 and 0.6PtO-TiO_2 photocatalysts are shown in Fig. 4c and d, respectively. In good agreement with XRD data, the crystallographic planes of both photocatalysts shown borders conforming to (101) and (110) planes (d_{101} = 0.35 nm and d_{110} = 0.32 nm) of the anatase (Ismail et al. 2010; Ismail and Bahnemann 2011). There are no changes in the lattice spacing of the anatase in the 0.6PtO-TiO_2 sample with respect to the pure TiO_2 which proves once more the absence of modifications in the TiO_2 lattice by doping with Pt ions. Additionally, the 0.6PtO-TiO_2 nanocomposite shows the well-defined lattice fringes of (111) crystalline

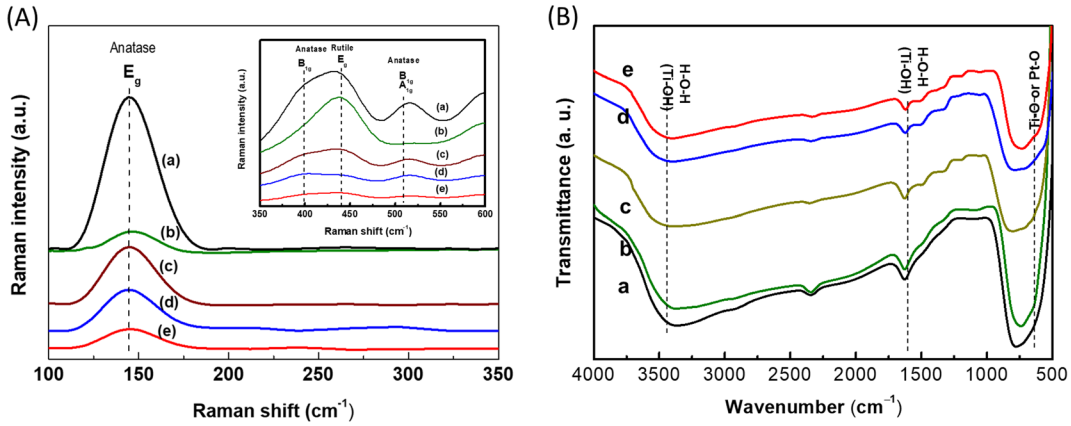

Fig. 2 Raman (A) and FTIR (B) spectra of pure TiO_2 (a) and *x*PtO-TiO_2 photocatalysts: 0.2PtO-TiO_2 (b), 0.4PtO-TiO_2 (c), 0.6PtO-TiO_2 (d), and 0.8PtO-TiO_2 (e)

planes with a distance of 0.21 nm characteristic of PtO nanocrystals. These nanocrystals have good contact with the TiO_2 surface, and they show the spherical shape and 5–7 nm in size (Jiang et al. 2016).

The chemical states of the *x*PtO-TiO_2 elements (represented by the 0.6PtO-TiO_2 sample) was examined by XPS. Figure 5a~c shows the Pt 4f, O 1s, and Ti 2p core spectra, respectively. The presence of Pt^{2+} ions in oxide environment can be deduced from the two crests at 72.5 eV and 75.9 eV experiential in the Pt $4f_{7/2}$ and Pt $4f_{5/2}$ core levels, singly (Fig. 5a) (Wang et al. 2018). On the other hand, the Ti 2p spectrum (Fig. 5b) consists of two summits at 458.0 and 464.0 eV associated with Ti $3d_{3/2}$ and Ti $3d_{5/2}$ core levels, respectively. Considering the former peak, the binding energy value at 458.0 eV is indicative of Ti^{4+} ions octahedrally coordinated in anatase TiO_2 phase (Acosta-Silva et al. 2013). The O 1s peak also corroborates the presence of TiO_2 at 530.0 eV which are due to oxygen ions in TiO_2 (Pretzer et al. 2008; Wang et al. 2009). The estimated PtO content in the TiO_2 by the XPS quantitative analysis is confirmed at 0.58%.

Figure 6a parades the UV-vis absorbance of the synthesized xPtO-TiO_2 photocatalysts. The absorbance spectra of the *x*PtO-TiO_2 trials are analogous to that presented by the pure TiO_2 due to the very low PtO loading on the surface of the TiO_2 (0.2–0.8 wt.%) (Jiang et al. 2016). As a consequence, all the *x*PtO-TiO_2 photocatalysts exhibit comparable light absorption ability. Noticeably, the *x*PtO-TiO_2 photocatalysts indicate a change of the beginning of the absorption edge toward extensive wavelengths concerning that of the pure TiO_2 suggesting modification in the bandgap energy (E_{bg}). The Tauc plot $((ahv)^{1/2}$ values against the photon energy) is publicized in the inlet of Fig. 6 and E_g values calculated using this Tauc plot are listed in Table 1. The E_g of mesoporous TiO_2 is 3.45 eV, whereas those of the *x*PtO-TiO_2 samples lie in the 2.5–2.55 eV range. The observed red move may accredit new levels of impurities generated in the bandgap of TiO_2 by the Pt orbitals from the PtO entities in close contact, at surface level, with TiO_2. Thus, it is clear that modification of mesoporous TiO_2 with PtO produces a surge in the light absorption capacity of the synthetized *x*PtO-TiO_2 in

Table 1 Physicochemical characterization of pure TiO_2 and xPtO-TiO_2 photocatalysts: specific surface area (S_{BET}), absorption edge (Abs. edge), band gap energies (E_g), PL emission peaks, and its corresponding photocatalytic destruction efficiency (ζ) of imazapyr herbicide within 150 min

Sample	S_{BET} (m^2/g)	Abs. edge (nm)	E_g (eV)	PL peaks (nm)	ζ(%)
TiO_2	170	384	3.45	385	1.0
0.2PtO-TiO_2	168	405	3.33	413	1.1
0.4PtO-TiO_2	164	429	2.95	437	4.7
0.6PtO-TiO_2	160	505	2.58	480	35.5
0.8PtO-TiO_2	155	507	2.55	477	35.9

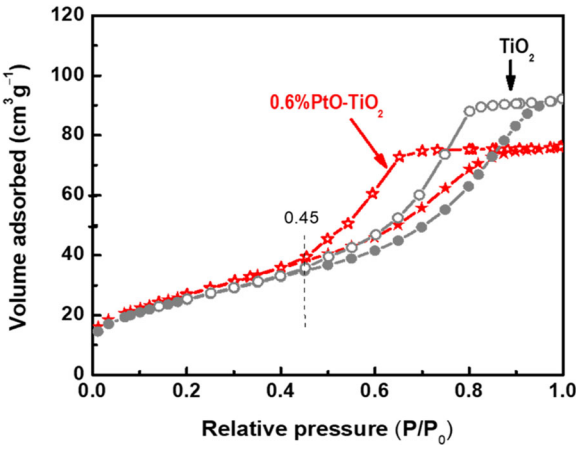

Fig. 3 Nitrogen adsorption-desorption isotherms of the pure TiO_2 and 0.6PtO-TiO_2 photocatalyst (adsorption and desorption data are represented by open and closed symbols, respectively)

good agreement with the previously published data (Uddin et al. 2005; Kim et al. 2014; Bamwenda et al. 1997).

Photocatalytic tests for Imazapyr degradation

Prior to photocatalytic tests, two reference trials were done to corroborate that the degradation of Imazapyr is only due to photocatalytic processes. The first blank experiment was carried out to appraise the possible photolysis of Imazapyr in the absence of photocatalyst. In contrast, the second one was performed to test the potential degradation of Imazapyr in the presence of the photocatalyst without illumination (data not shown here). The first blank experiment demonstrated that the lighting of Imazapyr herbicide during 150 min did not

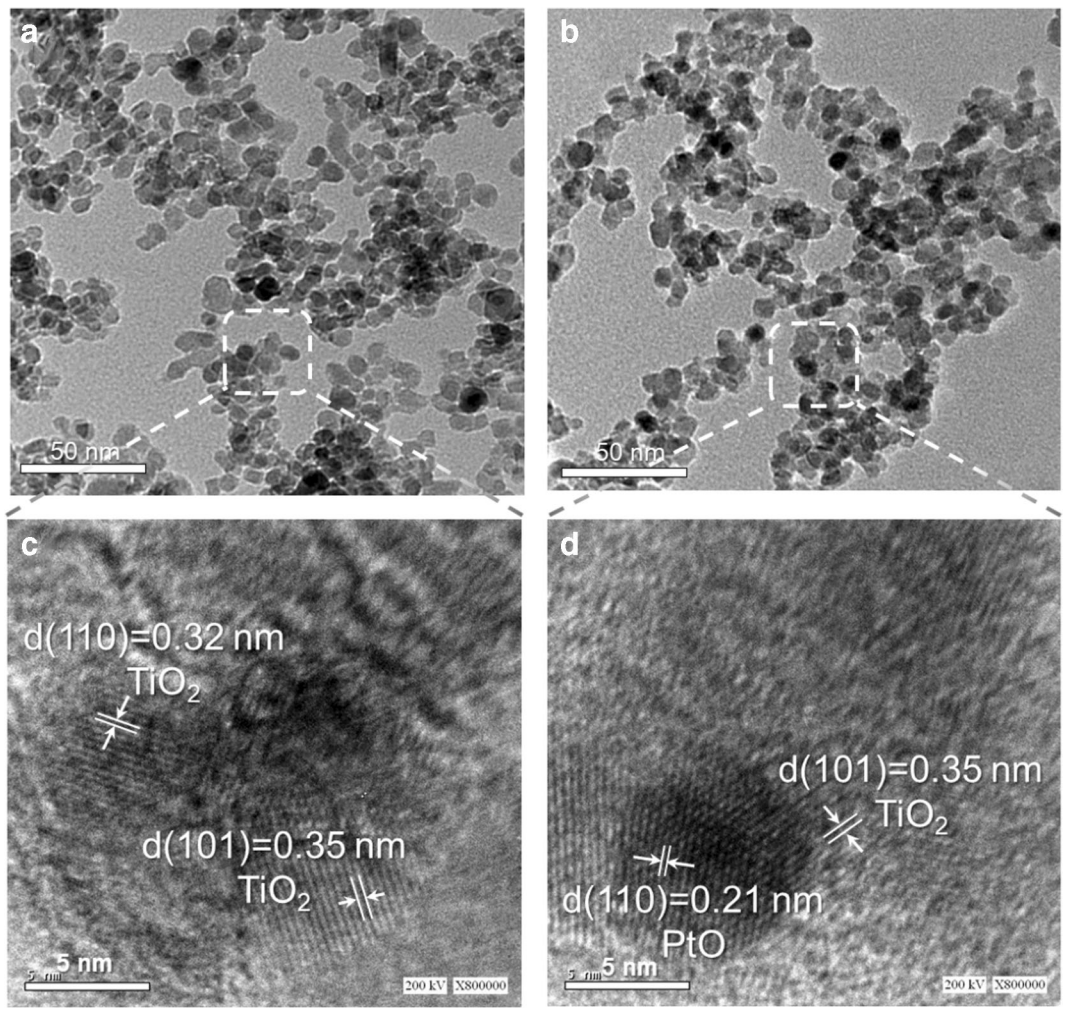

Fig. 4 TEM images of pure TiO_2 (**a**) and 0.6PtO-TiO_2 photocatalyst (**c**). HRTEM images showing lattice parameters for pure TiO_2 and 0.6PtO-TiO_2 are represented in (**c**) and (**d**), respectively

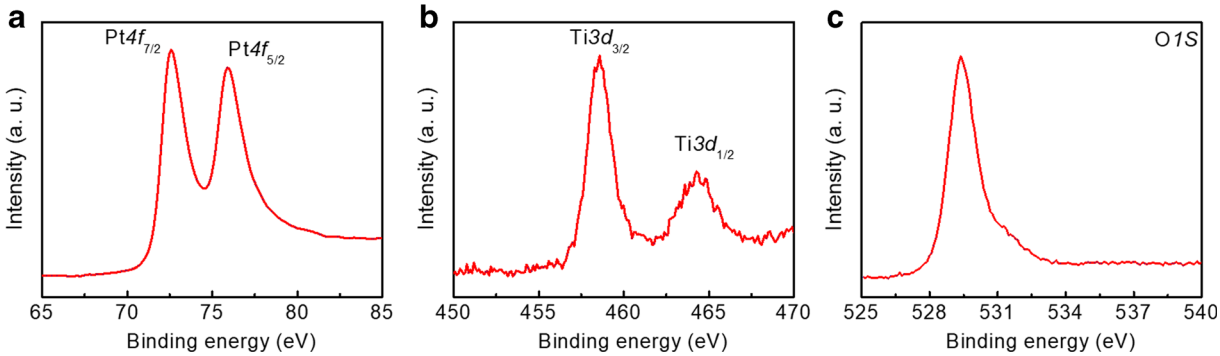

Fig. 5 X-ray photoelectron Pt 3d (**a**), Ti 2p (**b**), and O 1s (**c**) core level spectra of the 0.6PtO-TiO_2 photocatalyst

produce its photolysis. In contrast, the second blank experiment shown that the destruction of Imazapyr over mesoporous TiO_2 and *x*PtO-TiO_2 photocatalysts did not occur in the absence of light irradiation.

The photocatalytic efficacy of the pure TiO_2 and *x*PtO-TiO_2 samples was evaluated in the photooxidation of Imazapyr carried out at ambience under simulated solar light illumination. A commercial Degussa P25 was also tested as reference under the same reaction conditions. Figure 7a shows the percentage of herbicide degradation during 150 min of radiation time. The commercial Degussa P25 and pure mesoporous TiO_2 shows low photoactivity only degrading 4 and 10% of Imazapyr, respectively. The low activity demonstrated by these samples is related to the small UV component of the Xe lamp spectra used as a light source. Comparison of photoactivity on pure TiO_2 and *x*PtO-TiO_2 samples demonstrates the improvement in photoactivity in the samples modified with PtO. The best photocatalytic degradation of Imazapyr (about 99%) was archived over the photocatalysts containing 0.6 and 0.8 wt.% of PtO. The PtO-TiO_2 photocatalysts with lower PdO content, 0.2 and 0.4 wt%, are less active, showing about 40 and 80% of Imazapyr photooxidation after 150 min of irradiation time, respectively.

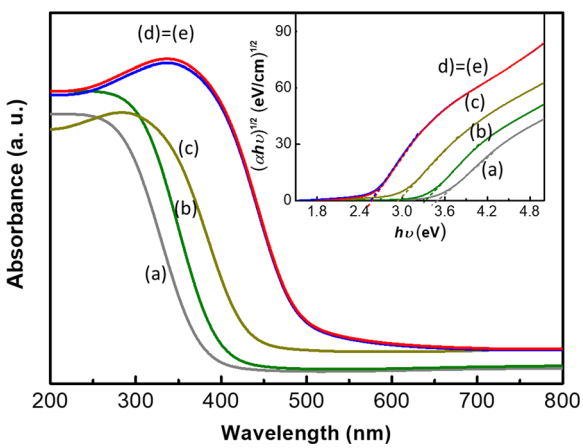

Fig. 6 UV-vis-NIR DRS of pure TiO_2 (**a**) and calcined 0.2PtO-TiO_2 (**b**), 0.4PtO-TiO_2 (**c**); 0.6PtO-TiO_2 (**d**), and 0.8PtO-TiO_2 (**e**) nanocomposites. Inset shown the estimation of band gap energy using Tauc plot

For all synthetized photocatalysts, the competence of photocatalytic procedures was evaluated by the extent of the photonic efficiency ζ (%), that is, the rate of the photodestruction of Imazapyr distributed by the incident photon flow, as expressed by the following equation (Ismail et al. 2010):

$$\xi = \frac{r \times 100}{I}$$

as *r* is Imazapyr photodestruction rate (mol L^{-1} s^{-1}) and *I* is the instance photon flow (6.26×10^{-7} Ein L^{-1} s^{-1}). For this equation, the primary photodegradation rate of Imazapyr degradation was calculated from the data presented in Fig. 7a through the initial 120 min of irradiation. The ζ values of the pure TiO_2 and *x*PtO-TiO_2 specimens are recorded in Table 1 and shown in Fig. 7b. The PtO-TiO_2 sample modified with 0.6 wt% of PtO exhibit the greatest ζ (35.5%) among the catalysts studied. The increase of PtO content from 0.6 to 0.8 wt% did not clue to an improvement in ζ (35.5% against 35.9%). The most active 0.6PtO-TiO_2 photocatalyst exhibits much greater photonic efficiency than pure mesoporous TiO_2 and commercial P25 Degussa reference photocatalysts (1% and 0.5%, respectively). For the most active 0.6PtO-TiO_2 photocatalyst, the mineralization of Imazapyr has been followed by measurement of the total organic carbon (TOC) after 6 h of irradiation time. The absence of traces of C suggests that this photocatalyst eliminated Imazapyr herbicide efficiently.

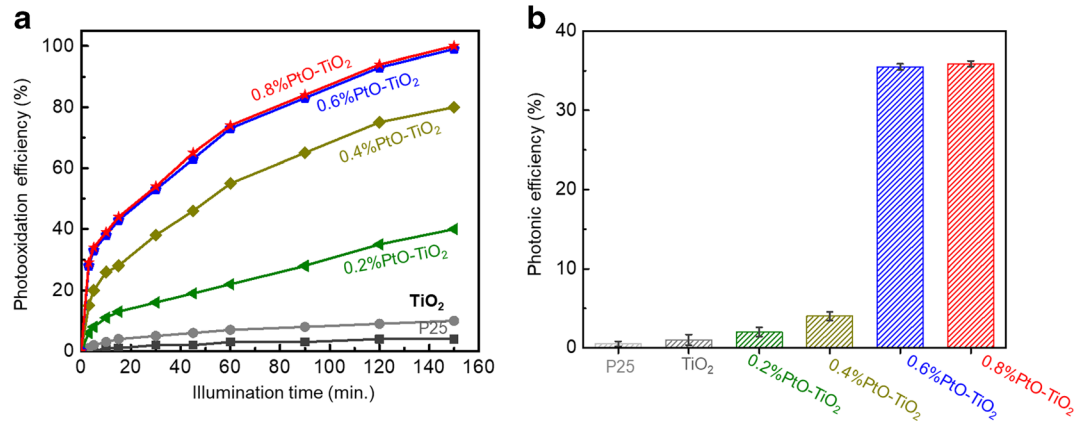

Fig. 7 Photooxidation efficiency of Imazapyr herbicide under simulated solar light (**a**) over mesoporous TiO_2, Degussa P25, and *x*PtO-TiO_2 photocatalysts. The corresponding photonic efficiency is shown in (**b**)

The optimum photocatalyst concentration needed for the maximum Imazapyr removal was evaluated using different concentrations (in the 0.5–2.5 g L^{-1} range) of the most active 0.6PtO-TiO_2 photocatalysts in the photoreactor (Fig. 8a). The results indicate that the best irradiation efficiency and accessibility to the photocatalyst particles for Imazapyr molecules were archived at 2.0 g L^{-1} photocatalyst concentration in the photoreactor. Photocatalysts concentration higher than this value led to a decrease in its photoefficiency due to the reduction of light available originated by the increase in the number of suspended catalyst particles (Mohamed et al. 2017; Mohamed 2009; Mohamed et al. 2012; Ismail et al. 2006; Mohamed et al. 2019; Mohamed and Salam 2014). Finally, the constancy and reuse of the optimized 0.6PtO-TiO_2 photocatalyst were evaluated by performing the photooxidation of Imazapyr during five consecutive runs (Fig. 8b). As seen in Fig. 8b, this most active 0.6PtO-TiO_2 photocatalyst preserved its photoefficiency for Imazapyr degradation up to five photocatalytic runs.

Photoluminescence and photocurrent measurements

The impact of PtO loading on the charge-carriers dynamics on PtO-TiO_2 photocatalysts was investigated by photoluminescence (PL) emission spectroscopy and photocurrent measurements. Figure 9a shows PL spectra of the photocatalysts excited at 365 nm. The spectrum of the bare TiO_2 shows the main emanation at 388 nm due to the bandgap electron-hole pair recombination. The PL emission intensities of all *x*PtO-TiO_2 photocatalysts decreases compared to the pure TiO_2 sample, ascending the emission intensities in the manner: 0.8PtO-TiO_2 = 0.6PtO-TiO_2 < 0.4PtO-TiO_2 < 0.2PtO-TiO_2 < TiO_2. The results from PL spectra demonstrated that all *x*PtO-TiO_2 photocatalysts show less intensity in the PL emissions respect to the pure TiO_2, which indicates the retarded chargerecombination. The position of the emission peaks also varies in the *x*PtO-TiO_2 photocatalysts respect to the bare TiO_2. The emission peaks of the *x*PtO-TiO_2 photocatalysts are red-shifted toward higher wavelength according to the sequence: 0.8PtO-TiO_2 = 0.6PtO-TiO_2 (557 nm) > 0.4PtO-TiO_2 (478 nm) > 0.2Pt-O-TiO_2 (416 nm) > TiO_2 (388 nm). As expected, the position of PL emission peak maxima are shifted toward higher wavelength values with the decrease of its energy band gap values.

The retarded recombination between electron and holes was also confirmed by photocurrent density measurements over the *x*PtO-TiO_2 photocatalysts under simulated solar light irradiation (Fig. 9b). In these measurements, the photocurrent density of the PtO-TiO_2 nanocomposites reduced in the following manner: 0.8PtO-TiO_2 > 0.6PtO-TiO_2 > 0.4PtO-TiO_2 > 0.2PtO-TiO_2 > TiO_2. Thus, the recombination between charge carriers is efficiently suppressed by the presence of PtO, in good agreement with the improvement in the photonic efficiency as the loading of PtO in the photocatalysts increases (Mohamed and Salam 2014; Mkhalid et al. 2020). This trend is the same as those of the photocatalytic performance, suggesting that transient photocurrent response is a main factor influencing on the photocatalyst photoeficiency. Indeed, it was found a linear correlation between the photocatalytic destruction efficiency and PL peak position (Fig. 10a). Taking into

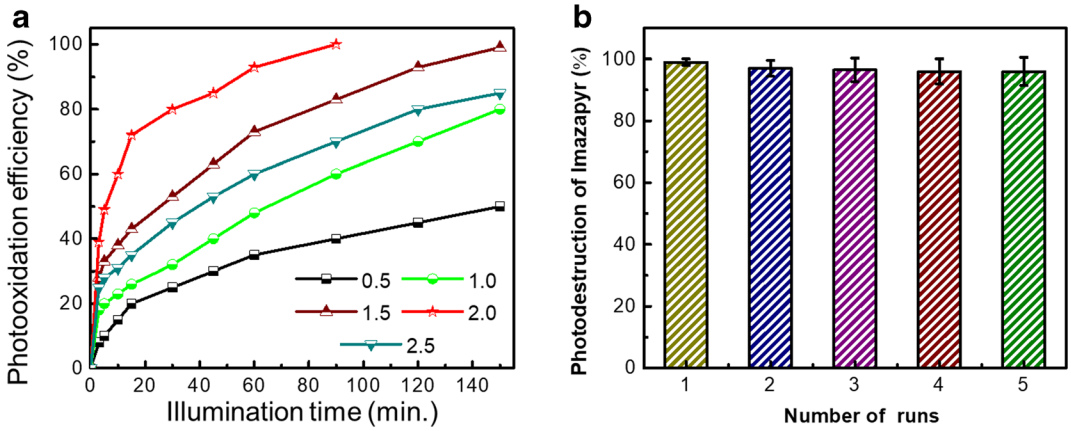

Fig. 8 Impact of the 0.6PtO-TiO_2 photocatalyst dose on the overall photooxidation of Imazapyr (**a**). Stability of this catalyst during five consecutive runs utilizing the optimized catalyst concentration (**b**)

account that PL peak position is related with the decrease of the E_g values of the photocatalysts (Fig. 10b), the rise in the visible light absorption capacity of the synthesized *x*PtO-TiO_2 could also participate in the improvement of photoactivity of the catalysts with the increase in the PdO loading.

Mechanism for Imazapyr degradation over xPtO-TiO_2 photocatalysts

As commented above, the improvement in the photoactivity of *x*PtO-TiO_2 photocatalysts was related with the close contact of PtO with the surface of the mesoporous TiO_2 that promoted a slight modification of the electronic band structure diminishing the band gap value and the charge carriers dynamics. The addition of PtO to mesoporousTiO_2 can improve its photoactivity thanks to the formation of close contacts with PtO that facilitates the spatial departure of electrons and holes. The relative position of the valence and conduction band of TiO_2 and PtO has been estimated from data published in the literature (Vijayan et al. 2010; Huang et al. 2010). According to these data, the VB and the CB of TiO_2 are placed at 2.8 and − 0.4 eV, respectively, whereas the bottom of the CB and the top of the VB of PtO are placed at 1.2 eV and − 0.4 eV, separately. The Fermi level (E_F) of PtO was higher than that of anatase TiO_2 and therefore an electric field was established from the interaction potential fences of PtO-TiO_2 (Jiang et al. n.d.). These contact potential barriers favors the transmission of photoelectrons from CB of TiO_2 to PtO enhancing the separation of photocharges, and thus higher photocatalytic efficiency is achieved because of the reduction of the recombination processes, as it was confirmed through the PL analysis (Fig. 9a, Fig. 10). Based on these results, a graphic depiction of the

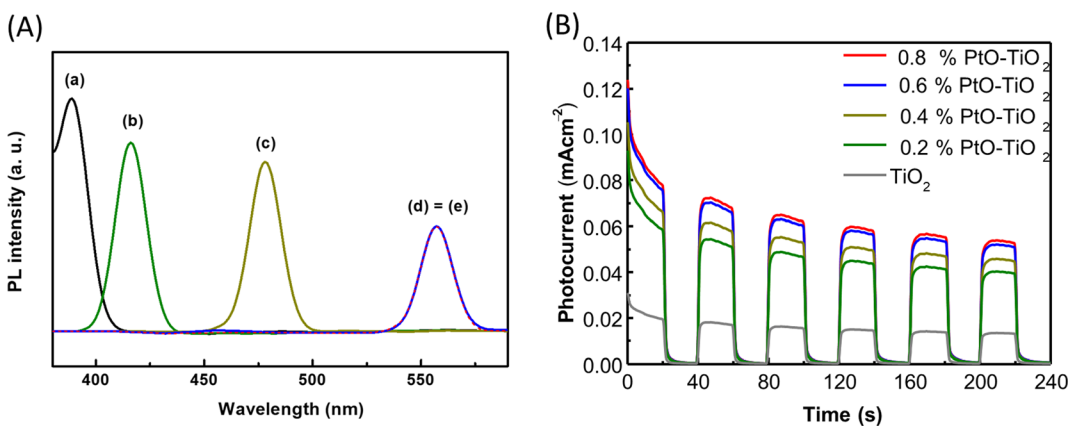

Fig. 9 Photoluminescence (PL) spectra (**a**) and transient photocurrent measurements (**b**) of the pure TiO_2 (a) and *x*PtO-TiO_2 photocatalysts, 0.2PtO-TiO_2 (b), 0.4PtO-TiO_2 (c), 0.6PtO-TiO_2 (d), and 0.8PtO-TiO_2 (e)

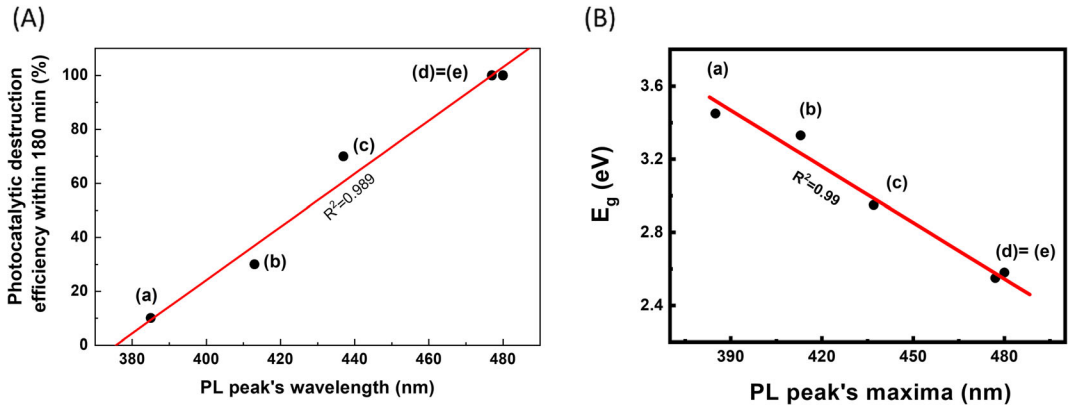

Fig. 10 Correlation between the photoxidation efficiency and PL peak position (**a**): (a) TiO_2 and *x*PtO-TiO_2 photocatalysts (b) 0.2PtO-TiO_2, (c) 0.4PtO-TiO_2, (d) 0.6PtO-TiO_2, and (e) 0.8PtO-TiO_2. Panle **b** shows the correlation between the energy band gap and PL emission peak's wavelength

possible procedure of the electron-hole separation operating on the *x*PtO-TiO_2 photocatalysts is presented in Fig. 11. In this scheme, the UV and visible light excited the *x*PtO-TiO_2 photocatalysts and led to the formation of charge carriers in the TiO_2 phase (Eq. 1). Then, the electrons transfer from the CB of TiO_2 to the conduction band of PtO occurs (Eq. 2), whereas the positive holes remain in the VB level of TiO_2 (Kim et al. 2005; Aarthi and Madras 2007).

$$\text{xPtO}-\text{TiO}_2 + h\nu \rightarrow \text{xPtO}-\text{TiO}_2(\text{CBe}^- + \text{VB}h^+) \quad (1)$$

$$\text{xPtO}-\text{TiO}_2(\text{CBe}^- + \text{VB}h^+) \rightarrow \text{PtO}(e^-)-\text{TiO}_2\ (h^+) \quad (2)$$

The excess of electrons on the CB of PtO might reduce the adsorbed molecular oxygen forming $O_2^{\bullet -}$ (Eq. 3), which via subsequent protonation might form $HO_2^{\bullet}$ radicals (Eq. 4) leading to the formation of hydrogen peroxide (Eqs. 5 and 6). The hydrogen peroxide molecules formed could be combined with additional electrons to generate the highly oxidizing $^{\bullet}OH$ radicals (Eqs. 7 and 8). Imazapyr herbicide can be destructed via oxidation with an oxidizing agent ($^{\bullet}OH$) and holes in TiO_2 leading to the formation of inert species (water and carbon dioxide) (Eqs. 9 and 10) (Aarthi and Madras 2007; Rajeshwar et al. 2008).

$$\text{PtO}(e^-) + O_2 \rightarrow \text{PtO} + O_2^{\bullet -} \quad (3)$$

$$O_2^{\bullet -} + H_2O \rightarrow HO_2^{\bullet} + {}^-OH \quad (4)$$

$$HO_2^{\bullet} + O_2^{\bullet -} + H_2O \rightarrow H_2O_2 + O_2 + {}^-OH \quad (5)$$

$$2HO^{\bullet}{}_2 \rightarrow H_2O_2 + O_2 \quad (6)$$

$$H_2O_2 + h\nu \rightarrow 2{}^{\bullet}OH \quad (7)$$

$$H_2O_2 + e^- \rightarrow {}^{\bullet}OH + {}^-OH \quad (8)$$

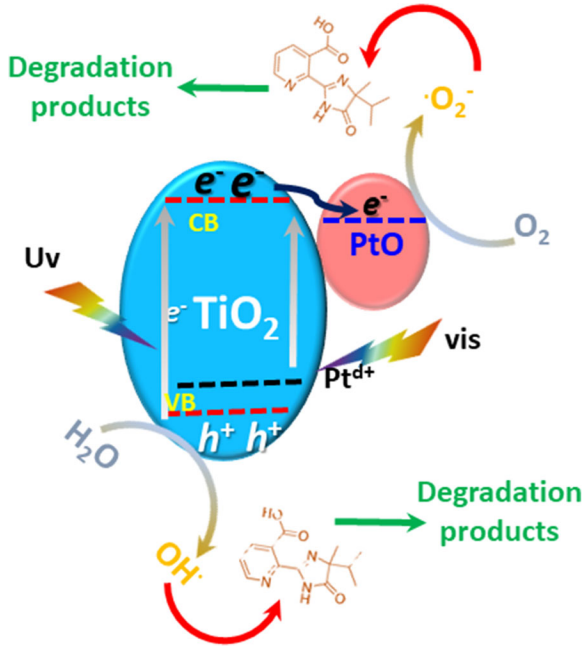

Fig. 11 Possible mechanism of the electron-hole separation during visible light irradiation on *x*PtO-TiO_2 photocatalysts

$$^{\bullet}OH + \text{Imazapyr} \rightarrow CO_2 + H_2O \quad (9)$$

$$TiO_2(h^+) + \text{Imazapyr} \rightarrow CO_2 + H_2O \quad (10)$$

Therefore, the improvement in the photoefficiency of the xPtO-TiO_2 photocatalysts with respect to the pure TiO_2 was related with the close contact of PtO with the surface of the mesoporous TiO_2. These contacts promoted a slight alteration of the band structure of TiO_2 diminishing the E_g value and promoting the efficient photoelectron separation, thereby increasing the efficiency in the photooxidation of Imazapyr.

Conclusions

In this work, we studied mesoporous xPtO-TiO_2 photocatalysts with different PtO loading synthetized by template-assisted sol-gel method. Physicochemical characterization revealed that the anatase structure and mesoporous characteristics of TiO_2 were maintained after the modification with PtO. Highly dispersed spherical PtO nanocrystals with good contact with the TiO_2 were observed on the xPtO-TiO_2 photocatalysts. The modification of TiO_2 with PtO produces an intensification in the light absorption capacity and improves the efficient photoelectron separation minimizing the charge carrier's recombination. These effects were determined by the PtO loading in the xPtO-TiO_2 photocatalysts becoming more intense as the concentration of Pt in the photocatalysts increases. The efficiency of mesoporous xPtO-TiO_2 photocatalysts for the Imazapyr degradation under visible light illumination depends on the PtO loading in the photocatalysts. The PtO-TiO_2 photocatalyst loaded with 0.6 wt.% of PtO possesses the greatest photonic efficiency toward destruction of Imazapyr herbicide. This photocatalyst demonstrated to be stable and recyclable after up to five consecutive catalytic runs. The higher photoefficiency of the PtO-TiO_2 photocatalysts was referred to the collaboration effect amid TiO_2 and the PtO leading to a considerable decrease of bandgap and lower recombination of excited carriers which translates into very effectual photocatalysts for the significant mineralization of Imazapyr herbicide below solar light radiation.

Acknowledgments This project was funded by the Deanship of Scientific Research (DSR) at King Abdulaziz University, Jeddah, Saudi Arabia under grant no. KEP-PhD-37-130-38. The authors, therefore, acknowledge with thanks DSR for technical and financial support.

Compliance with ethical standards

Conflict of interest The authors declare that they have no conflict of interest.

References

Aarthi T, Madras G (2007) Photocatalytic degradation of rhodamine dyes with nano-TiO_2. Ind Eng Chem Res 46:7–14

Acosta-Silva YJ, Nava R, Hernandez-Morales V, Macias-Sánchez SA, Pawelec B (2013) TiO_2/DMS-1 disordered mesoporous system: structural vharacteristics and methylene blue photodegradation activity. Microporous Mesoporous Mater 170:181–188

Atitar MF, Ismail AA, Bahneman D, Afanasev D, Emeline AV (2015) Mesoporous TiO_2 nanocrystals as efficient photocatalysts: impact of calcination temperatures and phase transformations on photocatalytic performances. Chem Eng J 264:417–424

Bamwenda GR, Tsubota S, Nakamura T, Haruta M (1997) The influence of the preparation methods on the catalytic activity of platinum and gold supported on TiO_2 for CO oxidation. Catal Lett 44:83–87

Cardenas-Lizana F, Gomez-Quero S, Idriss H, Keane MA (2009) Gold particle size effects in the gas-phase hydrogenation of *m*-dinitrobenzene over Au/TiO_2. J Catal 268:223–234

Faisal M, Khan SB, Rahman MM, Ismail AA, Asiri AM, Al-Sayari SA (2014) Development of efficient chemi-sensor and photocatalyst based on wet-chemically prepared ZnO nanorods for environmental remediation. J Taiwan Inst Chem Eng 45:2733–2741

Gregg SJ, Sing KSW (1982) Adsorption, surface area and porosity. Academic Press, London

Huang C, Wang I, Lin Y, Tseng Y, Lu C (2010) Visible light photocatalytic degradation of nitric oxides on PtOx-modified TiO_2 via sol–gel and impregnation method. J Mol Catal A Chem 316:163–170

Ishibai Y, Sato J, Akita S, Nishikawa T, Miyagishi S (2007) Photocatalytic oxidation of NOx by Pt-modified TiO_2 under visible light irradiation. J Photochem Photobiol A Chem 188: 106–111

Ismail AA, Bahnemann DW (2011) One-step synthesis of mesoporous platinum/titania nanocomposites as photocatalyst with enhanced its photocatalytic activity for methanol oxidation. Green Chem 13:428–435

Ismail AA, Ibrahim IA (2008) Impact of supercritical drying and heat treatment on physical properties of titania/silica aerogel monolithic and its applications. Appl Catal A Gen 346:200–205

Ismail AA, Bahnemann DW, Bannat I, Wark M (2009) Gold nanoparticles on mesoporous interparticle networks of

titanium dioxide nanocrystals for enhanced photonic efficiencies. J Phys Chem C 113:7429–7435

Ismail AA, Bahnemann DW, Robben L, Wark M (2010) Palladium doped porous titania photocatalysts: impact of mesoporous order and crystallinity. Chem Mater 22:108–116

Ismail AA, Abdelfattah I, Robben L, Bouzid H, Al-Sayari SA, Bahnemann DW (2015) Photocatalytic degradation of Imazapyr using mesoporous Al_2O_3-TiO_2 nanocomposites. Sep Purif Technol 145:147–153

Ismail AA, Mohamed RM, Fouad OA, Ibrahim IA (2006) Synthesis of nanosized ZSM-5 using different alumina sources. Crystal Research and Technology, 41(2):145–149

Ismail AA, Abdelfattah I, Helal A, Al-Sayari SA, Robben L, Bahnemann DW (2016) Ease synthesis of mesoporous WO_3-TiO_2 nanocomposites with enhanced photocatalytic performance under visible light and UV illumination. J Hazard Mater 307:43–54

Ismail AA, Abdelfattah I, Faisal M, Helal A (2018) Efficient photodecomposition of herbicide Imazapyr over mesoporous Ga_2O_3-TiO_2 nanocomposites. J Hazard Mater 342:519–526

Jiang J, Yu J, Cao S (2016) Au/PtO nanoparticle-modified g-C 3 N 4 for plasmon-enhanced photocatalytic hydrogen evolution under visible light. J Colloid Interface Sci 461:56–63

Jiang Z, Li J, Liao W, Fan G, Yu H, Chen L, Su Z (n.d.) Synthesis and characterization of the optical properties of Pt-TiO_2 Nanotubes. J Nanomater 2017:6759853

Jing D, Zhang Y, Guo L (2005) Study on the synthesis of Ni doped mesoporous TiO_2 and its photocatalytic activity for hydrogen evolution in aqueous methanol solution. Chem Phys Lett 415:74–78

Kibombo HS, Wu C-M, Peng R, Baltrusaitis J, Koodali RT (2013) Investigation of the role of platinum oxide for the degradation of phenol under simulated solar irradiation. Appl Catal B Environ 136-137:248–259

Kim S, Hwang SJ, Choi WY (2005) Visible light active platinum-ion-doped TiO_2 photocatalyst. J Phys Chem B 109:24260–24267

Kim W, Tachikawa T, Kim H (2014) Visible light photocatalytic activities of nitrogen and platinum-doped TiO_2: synergistic effects of co-dopants. Appl Catal B Environ 147:642–650

Kumaresan L, Prabhu A, Palanichamy M, Arumugam E, Murugesan V (2011) Synthesis and characterization of Zr^{4+}, La^{3+} and Ce^{3+} doped mesoporous TiO_2: evaluation of their photocatalytic activity. J Hazard Mater 186:1183–1192

Mkhalid IA, Fierro JLG, Mohamed RM, Alshahri AA (2020) Photocatalytic visible-light-driven removal of the herbicide imazapyer using nanocomposites based on mesoporous TiO_2 modified with Gd_2O_3. Appl Nanosci 10:3773–3786. https://doi.org/10.1007/s13204-020-01479-8

Mohamed RM (2009) Characterization and catalytic properties of nano-sized Pt metal catalyst on TiO_2-SiO_2 synthesized by photo-assisted deposition and impregnation methods. J Mater Process Technol 209(1):577–583

Mohamed RM, Aazam E (2013) Synthesis and characterization of P-doped TiO_2 thin-films for photocatalytic degradation of butyl benzyl phthalate under visible-light irradiation. Chin J Catal 34(6):1267–1273

Mohamed RM, Salam MA (2014) Photocatalytic reduction of aqueous mercury (II) using multi-walled carbon nanotubes/Pd-ZnO nanocomposite. Mater Res Bull 50:85–90

Mohamed RM, Mkhalid IA, Baeissa ES, Al-Rayyani MA (2012) Photocatalytic degradation of methylene blue by Fe/ZnO/SiO_2 nanoparticles under visible light. J Nanotechnol 2012: 1–5

Mohamed RM, Shawky A, Mkhalid IA (2017) Facile synthesis of MgO and Ni-MgO nanostructures with enhanced adsorption of methyl blue dye. J Phys Chem Solids 101:50–57

Mohamed RM, Mkhalid IA, Shawky A (2019) Facile synthesis of Pt–In_2O_3/$BiVO_4$ nanospheres with improved visible-light photocatalytic activity. J Alloys Compd 775:542–548

Nolan M (2011) Surface modification of TiO_2 with metal oxide nanoclusters: a route to composite photocatalytic materials. Chemical Communications 47(30):8617–8619

Pretzer LA, Carlson PJ, Boyd JE (2008) The effect of Pt oxidation state and concentration on the photocatalytic removal of aqueous ammonia with Pt modified titania. J Photochem Photobiol A Chem 200:246–253

Rajeshwar K, Osugi M, Chanmanee W, Chenthamarakshan C, Zanoni M, Kajitvichyanukul P, Krishnan AR (2008) Heterogeneous photocatalytic treatment of organic dyes in air and aqueous media. J Photochem Photobiol C Photochem Rev 9:171–192

Robben L, Ismail AA, Lohmeier SJ, Feldhoff A, Bahnemann DW, Buhl J-C (2012) Facile synthesis of highly ordered mesoporous and well crystalline TiO_2: Impact of different gas atmosphere and calcinations temperature on structural properties. Chem Mater 24:1268–1275

Sekiya T, Ohta S, Kamei S, Hanakawa M, Kurita S (2001) Raman spectroscopy and phase transition of anatase TiO_2 under high pressure. J Phys Chem Solids 62:717–721

Shannon RD (1976) Revised effective ionic radii and systematic studies of interatomic distances in halides and chalcogenides. Acta Crystallogr A32:751–767

Souza FL, Teodoro TQ, Vasconcelos VM, Migliorini FL, Lima Gomes PCF, Ferreira NG, Baldan MR, Haiduke RLA, Lanza MRV (2014) Electrochemical oxidation of Imazapyr with BDD electrode in titanium substrate. Chemosphere 117: 596–603

Streal M, Horner DJ (2000) Adsorption of highly soluble herbicides from water using activated carbon and hypercrosslinked polymers. Trans IChemE Part B 78:363–382

Tauc J, Grigorovici R, Vanuc A (1966) Electronic structure of amorphous germanium. Phys Status Solidi:15627–15637

Tayade RJ, Kulkarni RG, Jasra RV (2006) Transition metal ion impregnated mesoporous TiO_2 for photocatalytic degradation of organic contaminants in water. Ind Eng Chem Res 45: 5231–5238

Uddin J, Peralta JE, Scuseria GE (2005) Density functional theory study of bulk platinum monoxide. Phys Rev B 71:155112

Vargas S, Arroyo R, Haro E, Rodrguez R (1999) Effects of cationic dopants on the phase transition temperatures of titania prepared by the sol-gel method. J Mater Res 14: 3932–3937

Vijayan BK, Dimitrijevic NM, Wu J, Gray KA (2010) The effects of Pt doping on the structure and visible light photoactivity of titania nanotubes. J Phys Chem C 114:21262–21269

Wang H, Wu Z, Liu Y, Wang Y (2009) Influences of various Pt dopants over surface platinized TiO_2 on the photocatalytic oxidation of nitric oxide. Chemosphere 74:773–778

Wang C, Fan H, Ren X, Wen Y, Wang W (2018) Highly dispersed PtO nanodots as efficient co-catalyst for photocatalytic hydrogen evolution. Appl Surf Sci 462:423–431

Yang Y, Sugino O, Ohno T (2012) Band gap of β-PtO_2 from first-principles. AIP Adv 2(022172):1–8

Publisher's note Springer Nature remains neutral with regard to jurisdictional claims in published maps and institutional affiliations.